SCIENTIFIC REPORTS

OPEN

SUBJECT AREAS:
SOLAR CELLS
NANOPARTICLES

Received
20 September 2013

Accepted
29 November 2013

Published
17 December 2013

Correspondence and requests for materials should be addressed to D.K. (dongho@yonsei.ac.kr) or S.-Y.J. (syjang@kookmin.ac.kr)

Highly Efficient Plastic Crystal Ionic Conductors for Solid-state Dye-sensitized Solar Cells

Daesub Hwang[1,2], Dong Young Kim[2], Seong Mu Jo[2], Vanessa Armel[3], Douglas R. MacFarlane[3], Dongho Kim[1] & Sung-Yeon Jang[4]

[1]Department of Chemistry, Yonsei University, Seoul 120-749, Korea, [2]Optoelectronic Materials Lab, Korea Institute of Science and Technology, Seoul 136-791, Korea, [3]Australian Centre for Electromaterials Science, School of Chemistry, Monash University, Clayton, VIC 3800, Australia, [4]Department of Chemistry, Kookmin University, Seoul 136-702, Korea.

We have developed highly efficient, ambient temperature, solid-state ionic conductors (SSICs) for dye-sensitized solar cells (DSSCs) by doping a molecular plastic crystal, succinonitrile (SN), with trialkyl-substituted imidazolium iodide salts. High performance SSICs with enhanced ionic conductivity (2–4 mScm^{-1}) were obtained. High performance solid-state DSSCs with power conversion efficiency of 7.8% were fabricated using our SSICs combined with unique hierarchically nanostructured TiO_2 sphere (TiO_2-SP) photoelectrodes; these electrodes have significant macroporosity, which assists penetration of the solid electrolyte into the electrode. The performance of our solid-state DSSCs is, to the best of our knowledge, the highest reported thus far for cells using plastic crystal-based SSICs, and is comparable to that of the state-of-the-art DSSCs which use ionic liquid type electrolytes. This report provides a logical strategy for the development of efficient plastic crystal-based SSICs for DSSCs and other electrochemical devices.

Dye-sensitized solar cells (DSSCs) have attracted considerable attention due to their facile manufacturing process and relatively high energy-conversion efficiency at reasonable cost[1]. In particular, their good performance under low light intensity, and the ability to fabricate devices with various colors, supports their application as portable energy devices. In DSSCs, appropriate electrolytes that can regenerate dyes at sufficient rate are crucial for cell performance. Solvent-based electrolytes, typically containing the I^-/I_3^- redox couple, exhibit good ion-transport characteristics; high power conversion efficiency of the corresponding cells (11.3% in I^-/I_3^- containing electrolytes and 12.3% in cobalt-based electrolytes) has been reported[2,3]. However, liquid electrolytes have their own disadvantages; they require hermetic sealing, and it is difficult to build flexible devices, which limits their commercialization[4]. Thus, the development of efficient solid-state DSSCs has become a key step towards the use of DSSCs as practical energy-conversion devices.

Thus far, a few different types of materials have been used to develop solid-state DSSCs. Solid-state hole-transporting-materials have yielded practical solid-state DSSCs, however their electronic hole-transport ability was not as effective as the ion-transport ability of typical electrolytes. This fact has limited the thickness of the TiO_2 photoelectrode layer, and restricted cell efficiency to $<6\%$[5–7]. Addition of ionic salts into solid matrices has been a popular approach to prepare solid-state electrolytes. Polymers are attractive matrices because they have good mechanical properties and are easily fabricated into devices, but these polymer electrolytes (polymer/salt mixtures) show relatively low ionic conductivity ($\leq 10^{-6}$ Scm^{-1}) at ambient temperature, and are difficult to penetrate fully into the porous photoanode[8–10]. The ionic mobility of polymer electrolytes is largely associated with local segmental relaxations in the amorphous phase of the polymers; these segments are often not mobile enough to allow high conductivities. Therefore, the ionic conductivity of polymer electrolytes at room temperature (RT) is often too low for practical application in electrochemical devices[11]. Tactics to improve the ionic conductivity of polymer electrolytes have included the introduction of disordered structure[12–14], blending different polymers[8], and adding high dielectric-constant liquid solvents that can dissociate the salts efficiently to form gel electrolytes[15,16]. Although significant improvement in ion conductivity has been achieved by addition of organic solvents, polymer gel electrolytes which contain solvent have many of the shortcomings of liquid electrolytes[8,14–16]. High ionic conductivity has not yet been obtained in liquid-solvent-free polymer electrolytes[10,15]. Solid matrices which can dissociate the ions efficiently and also infiltrate the structure of the electrodes more effectively than polymer matrices should yield better solid-state electrolytes for DSSCs.

Succinonitrile (SN) is a unique organic plastic crystal, which is macroscopically solid-state at RT because of high lattice stability, and can offer good ion diffusivity on the addition of ionic dopants because of its high concentration of defects[17,18]. In organic plastic crystals, defects or vacancies are created by the rotational disorder of the molecules, and these defects support partial translational motion within the three-dimensional lattice. plastic crystal-based solid-state ionic conductors (SSICs) thus display sufficient ion transport to be applied in electrochemical devices. Thus far, two types of plastic crystals have been developed: ionic plastic crystals, which are formed by an appropriate choice of cation/anion combination; and non-ionic plastic crystals, which are doped with ionic salts[19–21]. SN is a non-ionic organic plastic crystal, which effectively dissolves various types of salts[19,22–24]. It forms a stable plastic crystal phase between 233 and 331 K, maintaining a body-centered cubic (bcc) structure and a stable solid-like appearance. In this phase, the molecules exist in three isomeric conformations: two (identical) *gauche* and one *trans* isomer; the *trans* isomers act as "impurities" that create defects in the lattice, and hence lead to high molecular diffusivity[25]. Doping SN with appropriate salts to achieve sufficient ion conductivity in a stable plastic solid phase is a plausible strategy to obtain effective SSICs for DSSCs. SN is a promising matrix because its chemical structure and polarity resemble those of popular liquid-state organic solvents such as acetonitrile, valeronitrile and glutaronitrile[26,27]. The facilitated mobility of ions in doped SN electrolytes was previously demonstrated using pulsed field NMR[28]. The strategy of using SN as a solid-state matrix to incorporate the desired salts has been used for various electrochemical devices, which display improved performance compared to devices containing similar polymer-based gel electrolytes[19,23,29–31]. However, the development of SSICs for DSSCs using plastic crystals is still in a very early stage. Grätzel and coworkers reported plastic crystal-based DSSCs in which conversion efficiency is as high as ~5% at AM 1.5 G one sun illumination[29]. Recently, our group improved the efficiency up to 7.6% by using novel hierarchical TiO_2 nanofiber/nanosphere-based photoelectrodes, which can considerably reduce charge recombination[26,32]. This result motivated us to further develop this class of materials by further understanding of the fundamental aspects of plastic crystal-based SSICs.

In this study, highly efficient plastic crystal-based SSICs for solid-state DSSCs were developed by doping SN with various trialkyl-substituted imidazolium iodides (1-alkyl-2,3-dimethylimidazolium iodides, DMAIIs) and iodine. Our DMAII-doped SNs (DMAII-SNs) displayed elevated conductivities (2.1–3.7 $mScm^{-1}$) and iodide diffusion coefficients (2.6–3.5 $\times 10^{-6}$ cm^2s^{-1} for I^-) at RT, while maintaining their macroscopic solid-state properties. These values are much higher than those of typical polymer electrolytes, and are as high as those of imidazolium-based ionic liquid electrolytes[8,33]. In this paper we consider fundamental issues in the development of efficient plastic crystal-based SSICs (including lattice stability and ion transport properties). The effects of the chemical structure of the imidazolium salts and the ratio of salts/SN on the physical properties of the resulting SSICs are investigated. High performance solid-state DSSCs are fabricated using the DMAII-SNs, in conjunction with unique hierarchically structured TiO_2 sphere photoelectrodes (TiO_2-SP) that contain significant portion of macropores to improve electrolyte infiltration[34–36]. Some of the solid-state DSSCs fabricated using our DMAII-SNs exhibited power conversion efficiency values of 8.2% at AM 1.5 G (70 $mWcm^{-2}$), which is significantly higher performance than reported previously for DSSCs using plastic crystal-based SSICs (5–6.5%)[37,38], or polymer electrolytes[39,40].

Results

The SSICs were prepared by mixing various organic iodides with SN, a polar molecular plastic crystal. SN acts as a polar matrix, effectively dissolving the organic dopants (organic iodide salts and iodine), which supply the I^-/I_3^- redox couple. The facilitated diffusion of I^-/I_3^- in SN was reported previously[23]. Alkyl-substituted imidazolium iodides were selected as the source of I^- because they have been widely used in non-volatile electrolytes for DSSCs due to their high ionic conductivity and thermal stability[33,41,42]. Their physical properties are largely influenced by the alkyl-substituents on the imidazolium cations; these substituents determine the van der Waals (vdW) interactions among cations and Coulombic interactions with the anion. For example, the viscosities at room temperature (RT) of 1-alkyl-3-methyl-imidazolium iodides decrease as the alkyl chain length becomes shorter; 1-hexyl-3-methylimidazolium iodide (HMII) > 1-butyl-3-methylimidazolium iodide (BMII) > 1-propyl-3-methylimidazolium iodide (PMII) because of the reduced vdW interactions between the cations. However, further shortening of the alkyl chain to 1,3-dimethylimidazolium iodide (DMII) or 1-ethyl-3-methylimidazolium iodide (EMII) solidifies the salts at RT, as a result of their high lattice Gibbs energies arising from the conformational rigidity of the smaller cations.

Inspired by the excellent properties of 1-alkyl-3-methyl-substituted imidazolium iodides (AMIIs, Fig. 1A) as non-volatile electrolytes for DSSCs[33,41,42], various AMIIs were chosen as the dopants for our first attempt at developing SSICs. The AMIIs and I_2 were mixed with liquefied SN at 70°C, and then cooled to RT. Solid-state mixtures could be obtained at lower degrees of doping (<2 mole % of AMIIs); however, the ionic conductivity of these samples was too low (~10^{-7} Scm^{-1}), because of the low ion concentration, for them to be effective SSICs. When the AMII concentration increased to >3 mole %, the mixture turned into liquid-state (Fig. 1B). Notably, even doping with solid AMIIs (EMII and DMII) resulted in liquid-state mixtures, indicating that there is a significant decrease in SN melting point with added salt. Dopant systems that can be incorporated into SN at sufficient concentration, while maintaining the plastic crystal phase stability, are critical for effective SSICs.

To achieve this goal, we chose 1-alkyl-2,3-dimethy-imidazolium iodides (DMAIIs, structures are shown in Fig. 1A) as the dopants. In these compounds, the 2-position hydrogen is substituted by a methyl group. The additional CH_3 group in DMAIIs can significantly reduce the rotational and conformational freedom, and thus facilitate the association among alkyl chains. This can overcome the loss of hydrogen-bonding interactions with anions, resulting in increased melting point and viscosity for the methyl-substituted compound[43,44]. Because of this behavior, we expect that plastic crystal phase of SN may remain stable, even at high doping levels of DMAIIs. Fig. 1B shows photos of the DMAII-SN based SSICs prepared in this study. The DMAII-SNs remained solids at RT, at doping levels of up to

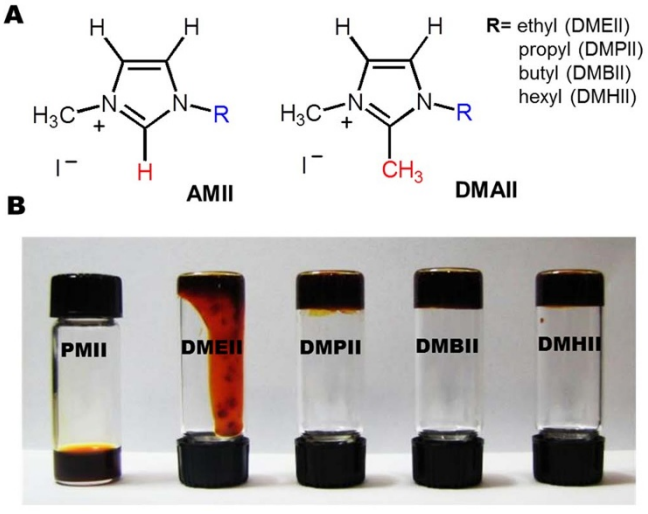

Figure 1 | (A) Molecular structures of the alkyl-substituted imidazolium iodide dopants, and (B) photo of plastic crystal-based SSICs.

6 mol.% DMAII (8 mol.% in the case of DMHII), with 1 mol.% of I_2. DMEII-SN was the exception, being a highly viscous liquid.

The thermograms of DMAII-SNs, measured by differential scanning calorimetry (DSC), are shown in Fig. S1 of the supporting information (SI). These DMAII-SN samples contained 6 mol.% DMAIIs (ethyl; DMEII, propyl; DMPII, butyl; DMBII, hexyl; DMHII) and 1% I_2. All the DMAII-SNs used in this study exhibited a plastic crystal phase at RT (Fig. S1), which indicates that 6 mol. % doping with DMAIIs does not significantly change the phase behavior of SN. This result indicated that the enhanced vdW interactions among imidazolium cations of DMAIIs provided significant rotational barriers and thus retard the disturbance of the plastic crystal lattice[45–47]. The enthalpy change that occurs during the normal solid-state to plastic crystal transition of DMAII-SNs (60–65 $J \cdot g^{-1}$) was similar to that of SN (pure plastic crystal) (73 $J \cdot g^{-1}$). The maximum amount of DMAII dopants that could be added into SN whilst maintaining the macroscopic solid plastic crystal phase at RT (ca. 293 K) were 4, 6, 6 and 8 mol.% for DMEII, DMPII, DMBII, and DMHII, respectively (refer to Fig. 1B).

Apart from solid-state stability, high ionic conductivity is another critical factor in the development of efficient SSICs. The ionic conductivities of our DMAII-SNs were obtained by measuring the impedance spectra of symmetric cells with Pt-coated FTO glass electrodes. Fig. 2 shows the σ values for DMAII-SNs at a range of temperatures. There was a transition in the ionic conductivity between as each electrolyte melted. The σ values of SN are known to be $10^{-8} \sim 10^{-6}$ Scm^{-1} in the plastic crystal phase (−30 to 58°C), with a corresponding activation energy (E_a) of 0.22 eV, arising from the trans-gauche dynamics[22,25]. Upon the addition of DMAIIs and iodine, the σ values at RT increased several orders of magnitude (to $\sim 10^{-3}$ Scm^{-1}, Fig. 2 and Table 1). These σ values are sufficient to build efficient DSSCs, and are superior to those previously reported for other plastic crystal-based SSICs[23,29], and some ionic-liquid-based non-volatile or quasi solid-state electrolytes that have been investigated[29,36,37]. As the alkyl chains of the DMAIIs became longer, the ionic conductivity decreased, because of increased interaction and interference between the ions[48–50]. Generally, the E_a values for ionic conduction in SN are reduced by the addition of salts, because the trans-gauche energy barrier is diminished by the enhanced microstructural disorder. However, a reduction in conformational dynamics can occur when the crystallinity is increased as a result of salt addition. The elevated E_a values for DMAII-SNs, compared to that of pure SN, indicate a significant reduction of conformational freedom upon the addition of DMAIIs. The values of ionic conductivity and activation energy are listed in Table 1; these were determined by fitting the conductivity data to the Arrhenius equation:

Table 1 | Conductivity parameters of DMAII-SNs

Sample	Activation Energy (eV, $kJmol^{-1}$)	Conductivity at RT ($mScm^{-1}$)
DMEII-SN	0.19, 18.7	3.7
DMPII-SN	0.32, 30.7	2.9
DMBII-SN	0.35, 34.6	2.6
DMHII-SN	0.36, 35.5	2.1

$$\sigma = A \cdot \exp(-E_a/RT) \quad (1)$$

where A is the pre-exponential factor and R is the gas constant.

The ion diffusion behavior of the DMAII-SN materials was investigated using steady-state voltammetry in a two-electrode electrochemical cell (Fig. 3). The ion diffusion coefficients of the redox couple species I^- and I_3^-, were calculated from the anodic and cathodic limiting currents by the following equation[51]:

$$D_{app} = I_{lim}/4nFCA \quad (2)$$

where D_{app} is apparent diffusion coefficient, I_{lim} is the anodic and cathodic steady-state limiting current, n is the electron number per molecule, F is the Faraday constant, C is the bulk concentration of electroactive species, and A is the radius of the Pt ultramicroelectrode. The diffusion coefficients of I^- and I_3^- in DMPII-SN were determined as 3.4×10^{-6} cm^2s^{-1} and 1.2×10^{-6} cm^2s^{-1}, respectively, which are higher than those of other reported plastic crystal-based SSICs[23], and ionic-liquid-based non-volatile or quasi solid-state electrolytes (1.9×10^{-7} cm^2s^{-1} and 3.1×10^{-7} cm^2s^{-1})[4,52].

In solid-state or quasi-solid-state electrolyte systems, the mass-transport of ions is retarded compared to that in liquid-state electrolytes. We hypothesize that the ion transport relies in these SN materials occurs mainly via a Grotthuss-type exchange mechanism (GEM), which requires much higher iodide/iodine ion concentration than typically found in liquid electrolyte solutions[53,54]. In the case of I_3^- diffusion, the formation of a sufficiently high concentration of polyiodide species can reduce the required mass diffusion distance down to ~the I−I bond length, 2.9 Å, and allows the GEM to operate, as shown in Fig. 4[53,55]. In the present case sufficient doping of the imidazolium salts (~6 mol. %) and iodine (~1 mol. %) into the SN matrix could enable efficient ion transport through the GEM, facilitated by the motion arising from crystal lattice defects. The optimum formulation for plastic crystal-based SSICs for DSSCs is one where high ion diffusion and macroscopic solid-state stability occur simultaneously. However, these requirements are not easily achieved, because the lattice defects within

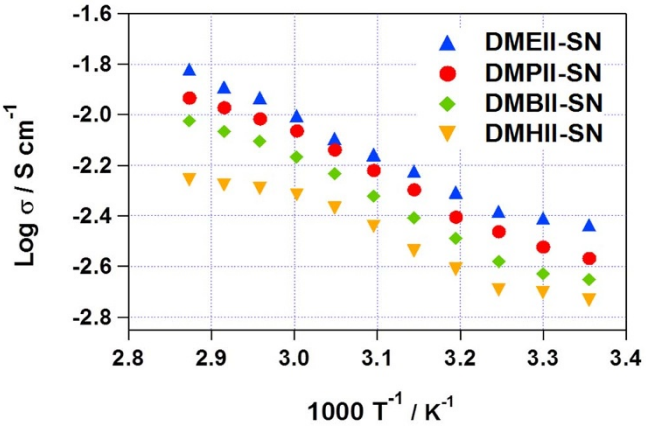

Figure 2 | Arrhenius plots of the conductivities of succinonitrile containing different DMAIIs (6 mol.%).

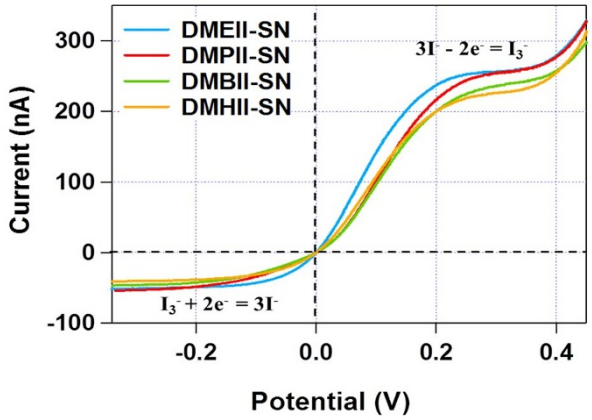

Figure 3 | Steady-state voltammograms of the DMAII-SNs obtained using a Pt ultramicroelectrode (radius = 5 μm) as the working electrode and a Pt foil as the counter electrode. The scan rate was 10 mVs^{-1}.

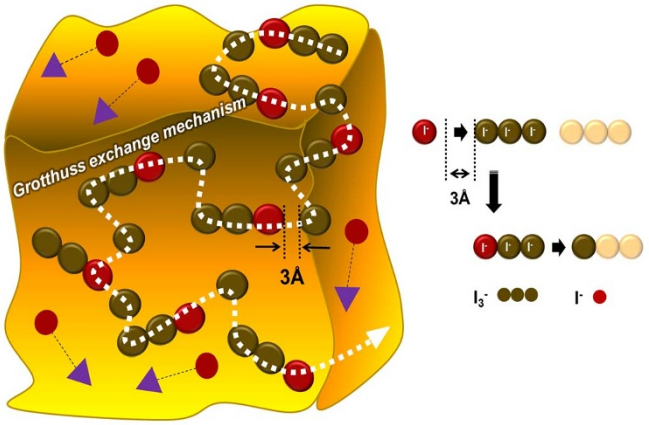

Figure 4 | Schematic illustration of ion transport, through a Grotthuss-type exchange mechanism, in our DMAII-SNs.

SN, which facilitate ion diffusion, diminish the lattice stability of the crystals. In our DMAII-SNs, the plastic crystal phase stability increased as the alkyl-substituents on the imidazolium salts became longer, but this then decreased the ion transport. After balancing these factors, DMPII-SN showed the highest ionic conductivity value (2.9 $mScm^{-1}$) and diffusion coefficient (3.4×10^{-6} cm^2s^{-1} for I^-) with sufficient macroscopic solid-state plastic crystal stability at RT. This makes DMPII-SN the most promising candidate for DMAII-SN-based SSICs.

Ambient temperature solid-state DSSCs containing the DMAII-SNs as SSICs, were fabricated as shown in Fig. 5. For the photoelectrodes, hierarchically-structured TiO_2-SP layers prepared by the electrospray method (as shown in Fig. S2) were used[56]. These TiO_2-SP electrodes have a significant portion of macropores (pore diameter ~100 nm), which is known to be beneficial for electrolyte infiltration, as reported previously[56]. Ru-based N719 dye was absorbed overnight onto the TiO_2-SP layers from an ethanolic solution. Thermolytically prepared Pt layers were used as cathodes. Finally, the molten DMAII-SNs at >70°C were injected into the pre-assembled cells, followed by cooling to RT. The detailed cell fabrication procedure is described in the experimental section.

Fig. 6A shows the photocurrent density-voltage (*J-V*) characteristics, under AM 1.5 G sunlight, of the solid-state DSSCs prepared using DMAII-SNs. All the devices displayed similar performance (as summarized in Table 3), however the DMPII-SN-based solid-state DSSC showed slightly higher efficiency because the relatively shorter propyl substituents promotes greater diffusional mobility than the longer alkyl substituents, with only minimal effects on the stability of resulting SSIC. Fig. 6B shows the impedance plane plots of solid-state DSSCs, the analysis of which are described in more detail in the supporting information (Fig. S3). The internal series resistance (R_S) of the device, as determined from the real component (Z') ranged from 30–50 Ωcm^2, while the resistance associated with diffusion (R_D), at the lowest frequency, was reduced as the alkyl-substituent length of the DMAIIs became shorter (Fig. 6 and Table 3). This result is consistent with the trends in ion conductivity and diffusion coefficient values for DMAII-SNs with various alkyl chain lengths (Tables 1 and 2) - in the case of I^-, 3.52×10^{-6} cm^2s^{-1} for DMEII-SN compared to 2.65×10^{-6} cm^2s^{-1} for DMHII-SN. As expected, the R_D values of the corresponding solid-state DSSCs (Table 3) exhibited the same trend (7.4 Ωcm^2 for DMEII-SN and 14.6 Ωcm^2 for DMHII-SN). Because the DMEII-SN is in a liquid-like state, the solid-state DSSCs using DMEII-SN showed the smallest R_D values and highest FF. However, their power conversion efficiency was lower than that of the DMPII-SN-based cells, because of their reduced V_{OC} value. As shown in the Bode phase plots (Fig. 6C), the peak frequency for the DMEII-SN-based cell was >10 Hz higher than those of the other DMAII-SN-based cells; this indicates that there is greater charge recombination on the TiO_2 photoelectrodes in the DMEII-SN-based cell, possibly because of the enhanced diffusion of I_3^- ions in the liquid-like DMEII-SN. It is intriguing that conversion efficiencies of solid-state DSSCs using our plastic crystal-based SSICs, in which the ions are transported by the GEM, were higher than that of the DSSC with the liquid electrolyte. Although DMHII-SN showed the most sluggish ion-transport, the corresponding solid-state DSSCs showed reasonable cell performance, with much enhanced solid-state stability. The cell performance results indicate that our DMAII-SNs are high-performance SSICs for DSSCs, and that our approach to design of the structures of plastic crystal-based SSICs for electrochemical devices has been effective.

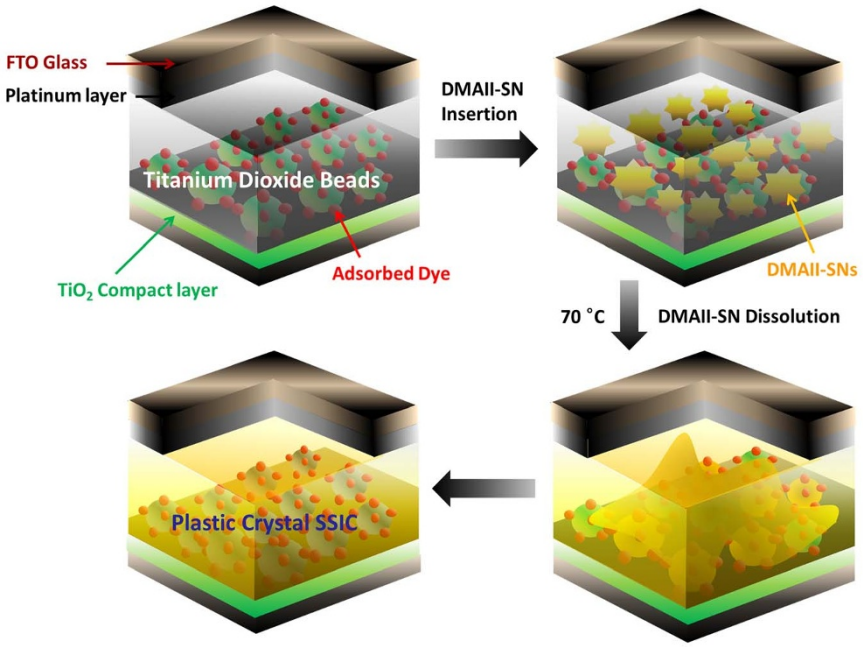

Figure 5 | Schematic illustration of the process for fabrication of solid-state DSSCs using TiO_2-SP photoelectrodes and DMAII-SN-based SSICs.

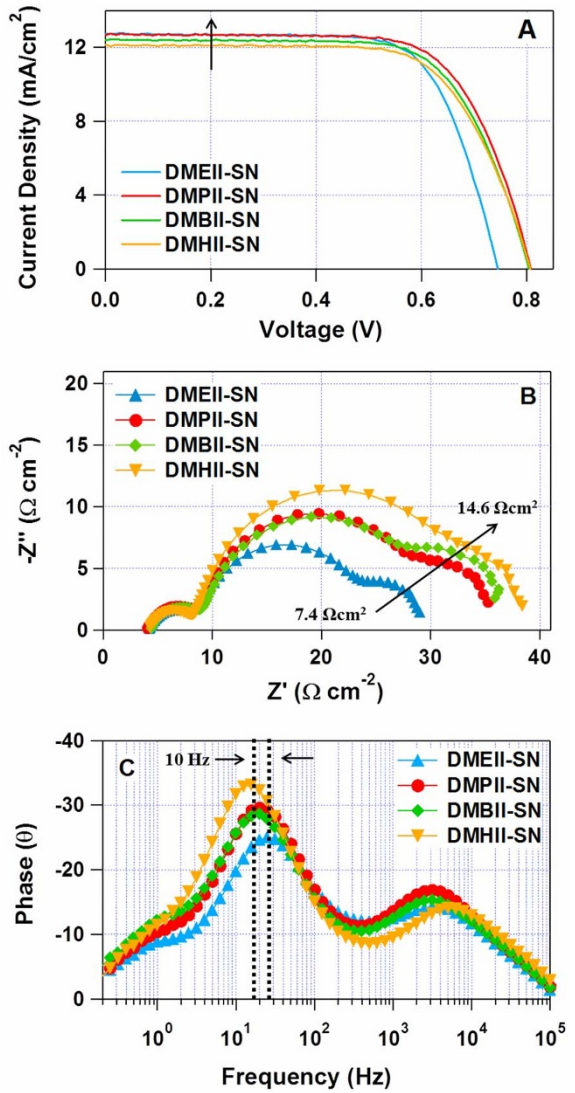

Figure 6 | (A) Photovoltaic performance; and EIS analysis results for the DMAII-SN-based solid-state DSSC at open-circuit conditions under simulated AM 1.5 G illumination; (B) Impedance plane plots for the frequency range 10^{-1}–10^5 Hz; (C) corresponding Bode phase plots.

To reveal the potential of our SSICs, we further optimized the solid-state DSSC using DMPII-SN by optimizing the thickness of the TiO_2-SP and the concentration of additives. The effects of the additive compositions on the cell performance were shown in Figure S4 ~ 8 and Table S2 ~ 3 in the SI). When ~13 μm thick TiO_2-SP photoelectrodes with the optimized additive composition were used, the *J*sc value improved to 15.4 mAcm^{-2}, and the power conversion efficiency reached ~7.8% (one sun illumination) with V_{OC} and *FF* of 725 mV and 69.9%, respectively. The *J-V* characteristics of the optimized solid-state DSSC under AM 1.5 G at various light intensities are shown in Fig. 7, and the resulting cell parameters are listed in Table 4. These efficiencies are significantly higher than those reported for other solid-state DSSCs using other plastic crystal electrolytes (<6.5%)[29] or ionic-liquid-based quasi-solid-state electrolytes[4,52–54]. Recently, our group reported highly efficient solid-state DSSCs which used N-methyl-N-butylpyrrolidinium iodide (P_{14}-I) doped SN as the plastic crystal electrolyte, and macroporous TiO_2 nanofibers as the photoelectrode. The conversion efficiency was 6.5% (AM 1.5 G, 100 mWcm^{-2}), the highest reported for cells using plastic crystal electrolytes. In the present work, the maximum efficiency value obtained was 8.2%, with V_{OC} of 727 mV, *J*sc of 11.0 mAcm^{-2}, and *FF* of 71.2% under optimized sunlight (70 mWcm^{-2} at AM 1.5 G). This value is even comparable to the state-of-the-art DSSC using the champion ionic-liquid-type electrolyte, as reported by Bai and coworkers[41], confirming the outstanding properties of the DMAII-SN electrolytes.

Table 2 | Ion diffusion coefficients in DMAII-SNs at T = 25°C

	Diffusion Coefficient	
Sample	$I^-/10^{-6}$ cm^{2}s^{-1} (0.62–0.64 M)	$I_3^-/10^{-6}$ cm^{2}s^{-1} (0.11 M)
DMEII-SN	3.52	1.18
DMPII-SN	3.43	1.18
DMBII-SN	2.73	0.96
DMHII-SN	2.65	0.73

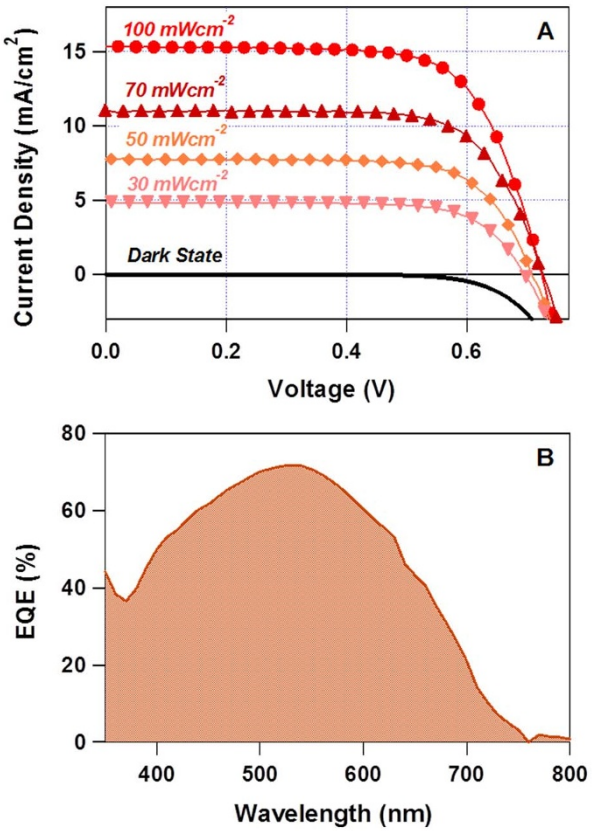

Figure 7 | Photovoltaic performance of solid-state DSSCs using DMPII-SNs. (A) *J-V* characteristics under the condition of simulated AM 1.5 G solar radiation at various light intensities; (B) Incident photon-to-current conversion efficiency (IPCE) spectra.

Discussion

We have developed highly efficient SSICs for solid-state DSSCs by doping a non-ionic plastic crystal, SN, with trialkyl-substituted imidazolium-iodide-based organic salts. The chemical structures and doping levels of the salts strongly influenced the stability of plastic crystal phase and the ion diffusion characteristics. A balance between the lattice motion and phase stability achieved outstanding ion-diffusion properties with good solid-state stability. The performance of the solid-state DSSCs reflected the useful properties of our DMAII-SNs, yielding the highest conversion efficiency ever reported for a DSSC using either a plastic crystal or quasi-solid-state electrolyte. The optimized cell efficiency of these solid-state DSSCs was 7.8%

Table 3 | Summary of the current-voltage (*J-V*) characteristics and EIS parameters of the three DSSCs, as determined by fitting the experimental data to the equivalent circuit shown in Fig. S3

DSSC	V_{OC} (mV)	J_{SC} (mA/cm^2)	*FF* (%)	η (%)	R_S ($\Omega\cdot$cm^2)	R_{Pt} ($\Omega\cdot$cm^2)	R_{CT} ($\Omega\cdot$cm^2)	R_D ($\Omega\cdot$cm^2)	R_{total} ($\Omega\cdot$cm^2)
DMEII-SN	745	12.72	71.4	6.8%	4.5	3.2	14.7	7.4	29.8
DMPII-SN	808	12.67	69.9	7.2%	4.6	3.1	20.3	8.5	36.5
DMBII-SN	804	12.40	69.3	6.9%	4.8	3.1	21.4	12.3	41.4
DMHII-SN	806	12.31	68.2	6.7%	4.8	3.0	24.9	14.6	47.3

(100 mWcm^{-2} at AM 1.5 G), comparable to that of state-of-the-art DSSCs using ionic liquid electrolytes. We believe that our work demonstrates a universal approach to effective design of plastic crystal-based SSICs for DSSCs. The core strategies outlined here can also be adapted for development of SSICs for other electrochemical devices.

Methods

Preparation of hierarchically structured TiO_2-SPs. 10 wt % P-25(Degussa) nanocrystalline-TiO_2 was dispersed in ethanol using an ultra apex mill (Model UAM-015, Kotobuki). The dispersed solution was loaded into a plastic syringe which was connected to a high voltage power supply (BERTAN SERIES 205B). Then, the dispersed P25 solution was electrosprayed directly onto conducting FTO substrates (10 × 10 cm). To prepare the hierarchically-structured TiO_2 spheres with a diameter of about 650 nm, an electric field of 15 kV was applied between the metal orifice and the conducting substrate. The feed rate was controlled by a syringe pump at 35–30 μl/min. To form a uniform thickness over a large area, the nozzle and the substrate were placed on a motion control system which was equipped with a microprocessor. More details and schemes of e-spray methods are described in the supporting information (Fig. S2).

Characterization of DMAII-SN-based SSICs. Differential scanning calorimetric scans were obtained to investigate the phase behavior of the plastic crystal electrolytes. The thermograms were measured with a Q2000 (TA instruments) at a heating rate of 10°C min^{-1}. The ionic conductivity of the plastic crystal electrolytes and its temperature dependence were determined by impedance measurements. The electrolyte was sandwiched between two mirror-finished stainless steel electrodes using a Teflon ring spacer in a constant-volume cylindrical cell, and was sealed with paraffin film in the glovebox. The sealed cell was maintained at various constant temperatures for at least 1 h prior to each measurement. The conductivity was calculated from the bulk resistance. To measure the steady state voltammograms for the electrolyte, a double-compartment electrochemical cell equipped with a 5.0 μm radius Pt ultramicroelectrode as the working electrode, a Pt foil as the counter electrode, and a Pt wire in the electrolyte as the reference electrode was used at a scan rate of 10 mV/s.

Device fabrication. For the working electrode, the TiO_2 films (~13 μm thick) were rinsed with water, and then sintered at 450°C for 30 min, after post-treatment with 0.05 M $TiCl_4$ for 20 min at 80°C. The TiO_2 electrodes were immersed into a purified 3 × 10^{-4} M *cis*-di(thiocyanato)-*N,N′*,bis(2,2′-bipyridyl-4-carboxylic acid-4′-tetrabutyl ammonium carboxylate) ruthenium (II) (N719, Solaronix) solution for 15 h at room temperature. For the counter electrode, the FTO plates were drilled using a microdrill, washed with 0.1 M HCl solution in ethanol, and then subsequently cleaned in an ultrasonic bath with water and ethanol for 15 min. A Pt counter electrode was prepared by drop casting 5 mM H_2PtCl_6 in isopropyl alcohol onto the washed FTO plates and then sintering the plates at 400°C for 20 min under air. The dye-adsorbed TiO_2 electrodes were rinsed with ethanol and dried under nitrogen flow, before being assembled and sealed with the counter electrode using thermal adhesive film (Surlyn, Dupont 1702, 25-μm-thick) as spacer to produce sandwich-type cells. The plastic crystal electrolyte, which consisted of succinonitrile, iodine (I_2), 1-alkyl-2,3-dimethylimidazolium iodides (DMAIIs), and N-methylbenzimidazole (NMBI) in a 100:1:6:0.5 (mole ratio), was introduced at 70°C through the hole drilled in the counter electrode. Finally, the holes were sealed with hot-melt film and a cover glass.

Table 4 | Summary of the *J-V* analysis of the optimized DMPII-SN-based solid-state DSSCs

Light Intensity	V_{OC} (mV)	J_{SC} (mA/cm^2)	*FF* (%)	η (%)
100 mWcm^{-2}	725	15.4	69.9	7.8%
70 mWcm^{-2}	727	11.0	71.2	8.2%
50 mWcm^{-2}	708	7.7	72.9	8.0%
30 mWcm^{-2}	697	4.8	72.8	8.2%

Photovoltaic & photoelectrical measurements. Photovoltaic measurement of the DSSCs employed an AM 1.5 solar simulator between the sample and a 450 W Xe lamp. The intensity of the simulated light was calibrated by a Si reference solar cell equipped with a BK7 filter to approximate AM 1.5 global radiation. The photovoltaic characteristics of the DSSC were obtained by applying an external potential bias to the cells and measuring the photocurrent generated with a Keithley model 2400 source meter. The photovoltaic performance was measured using black tapes with an aperture area of 0.25 cm^2. IPCE was measured as a function of wavelength from 350–800 nm using a specially designed IPCE system for dye-sensitized solar cells (PV measurement, Inc.). A 75 W xenon lamp was used as the light source to generate a monochromatic beam. Calibration was performed using a NIST-calibrated silicon photodiode as a standard. IPCE values were collected at a low chopping speed of 5 Hz. The electrical impedance spectra were measured using an impedance analyzer (Solatron 1260) at open-circuit potential under AM 1.5 full sun illumination (100 mWcm^{-2}), over a frequency range of 0.1–10^5 Hz. The magnitude of the alternating signal was 10 mV. Impedance parameters were determined by fitting the impedance spectra using Z-plot software.

1. O'Regan, B. & Grätzel, M. A Low-Cost, High-Efficiency Solar-Cell Based on Dye-Sensitized Colloidal TiO_2 Films. *Nature* **353**, 737–740 (1991).
2. Brian, E. H., Henry, J. S. & Michael, D. M. The renaissance of dye-sensitized solar cells. *Nat. Photonics* **6**, 162–169 (2012).
3. Aswani, Y. *et al.* Porphyrin-Sensitized Solar Cells with Cobalt (II/III)–Based Redox Electrolyte Exceed 12 Percent Efficiency. *Science* **334**, 629–634 (2011).
4. Peng, W. *et al.* Gelation of Ionic Liquid-Based Electrolytes with Silica Nanoparticles for Quasi-Solid-State Dye-Sensitized Solar Cells. *J. Am. Chem. Soc.* **125**, 1166–1167 (2003).
5. Henry, J. S. *et al.* Efficiency Enhancements in Solid-State Hybrid Solar Cells via Reduced Charge Recombination and Increased Light Capture. *Nano Lett.* **7**, 3372–3376 (2007).
6. Francisco, F.-S. *et al.* Correlation between Photovoltaic Performance and Impedance Spectroscopy of Dye-Sensitized Solar Cells Based on Ionic Liquids. *J. Phys. Chem. C* **111**, 6550–6560 (2007).
7. Ning, C. *et al.* An Organic D-π-A Dye for Record Efficiency Solid-State Sensitized Heterojunction Solar Cells. *Nano Lett.* **11**, 1452–1456 (2011).
8. Jilian, N. D. F. *et al.* New insights into dye-sensitized solar cells with polymer electrolytes. *J. Mater. Chem.* **19**, 5279–5294 (2009).
9. Li, W. *et al.* A 7.72% efficient dye sensitized solar cell based on novel necklace-like polymer gel electrolyte containing latent chemically cross-linked gel electrolyte precursors. *Chem. Comm.* **45**, 5687–5689 (2005).
10. Jian-Ging, C. *et al.* In Situ Low Temperature Polymerization of Bismaleimide for Gel-Type Electrolyte for Dye-Sensitized Solar Cells. *J. Phys. Chem. C* **114**, 13832–13837 (2010).
11. Dongmei, L. *et al.* Optimization the solid-state electrolytes for dye-sensitized solar cells. *Energy Environ. Sci.* **2**, 283–291 (2009).
12. Alasdair, M. C. *et al.* Increasing the conductivity of crystalline polymer electrolytes. *Nature* **433**, 50–53 (2005).
13. Bongha, S. *et al.* Barrier effect of dendrons on TiO_2 particles in dye sensitized solar cells. *Chem. Comm.* **47**, 1734–1736 (2011).
14. Donald, A. T. *et al.* Starburst-Dendrimere: Kontrolle von Gröe, Gestalt, Oberflächenchemie, Topologie und Flexibilität beim Übergang von Atomen zu makroskopischer Materie. *Angew. Chem.* **102**, 119–157 (1990).
15. Dong-Won, K. *et al.* Photovoltaic performance of dye-sensitized solar cell assembled with gel polymer electrolyte. *J. Power Sources* **149**, 112–116 (2005).
16. Peng, W. *et al.* A stable quasi-solid-state dye-sensitized solar cell with an amphiphilic ruthenium sensitizer and polymer gel electrolyte. *Nat. Mater.* **2**, 402–407 (2003).
17. Bischofberger, T. & Courtens, E. Optical Kerr Effect, Susceptibility, and Order Parameter of Plastic Succinonitrile. *Phys. Rev. Lett.* **32**, 163–166 (1974).
18. Derollez, P. *et al.* Structure of succinonitrile in its plastic phase. *J. Phys.: Condens. Matter* **2**, 6893–6903 (1990).
19. Pierre-Jean, A. *et al.* The plastic-crystalline phase of succinonitrile as a universal matrix for solid-state ionic conductors. *Nat. Mater.* **3**, 476–481 (2004).
20. Douglas, R. M. *et al.* Pyrrolidinium Imides: A New Family of Molten Salts and Conductive Plastic Crystal Phases. *J. Phys. Chem. B* **103**, 4164–4170 (1999).
21. Jennifer, M. P. *et al.* Organic ionic plastic crystals: recent advances. *J. Mater. Chem.* **20**, 2056–2062 (2010).

22. Supti, D. *et al.* Study of Ion Transport in Lithium Perchlorate-Succinonitrile Plastic Crystalline Electrolyte via Ionic Conductivity and in Situ Cryo-Crystallography. *J. Phys. Chem. B* **113**, 5025–5031 (2009).
23. Qing, D. *et al.* Rapid Diffusion in a Molecular-Plastic-Crystal Electrolyte for Potential Application in Solid-State Photoelectrochemical Cells. *Angew. Chem.* **44**, 313–316 (2005).
24. Li-Zhen, F. *et al.* Succinonitrile as a Versatile Additive for Polymer Electrolytes. *Adv. Func. Mater.* **17**, 2800–2807 (2007).
25. Hawthorne, H. M. & Sherwood, J. N. Lattice defects in plastic organic crystals. Part 3.-Plastic deformation in pure and impure camphene. *Trans. Faraday Soc.* **66**, 1790–1801 (1970).
26. Daesub, H. *et al.* High-Efficiency, Solid-State, Dye-Sensitized Solar Cells Using Hierarchically Structured TiO_2 Nanofibers. *ACS Appl. Mater. Interfaces* **3**, 1521–1529 (2011).
27. Vanessa, A. *et al.* Ionic liquid electrolyte porphyrin dye sensitised solar cells. *Chem. Comm.* **46**, 3146–3148 (2010).
28. Long, S. *et al.* Fast ion conduction in molecular plastic crystals. *Solid State Ionics* **161**, 105–112 (2003).
29. Peng, W. Ambient Temperature Plastic Crystal Electrolyte for Efficient, All-Solid-State Dye-Sensitized Solar Cell. *J. Am. Chem. Soc.* **126**, 13590–13591 (2004).
30. Monalisa, P. & Aninda, J. B. Plastic-polymer composite electrolytes: Novel soft matter electrolytes for rechargeable lithium batteries. *Electrochem. Commun.* **10**, 1912–1915 (2008).
31. Vanessa, A. *et al.* Organic ionic plastic crystal electrolytes; a new class of electrolyte for high efficiency solid state dye-sensitized solar cells. *Energy Environ. Sci.* **4**, 2234–2239 (2011).
32. Daesub, H. *et al.* Superior photoelectrodes for solid-state dye-sensitized solar cells using amphiphilic TiO_2. *J. Mater. Chem. A* **1**, 1228–1238 (2013).
33. Zhipan, Z. *et al.* The 2,2,6,6-Tetramethyl-1-piperidinyloxy Radical: An Efficient, Iodine- Free Redox Mediator for Dye-Sensitized Solar Cells. *Adv. Func. Mater.* **19**, 2187–2202 (2009).
34. Daesub, H. *et al.* Electrospray preparation of hierarchically-structured mesoporous TiO_2 spheres for use in highly efficient dye-sensitized solar cells. *ACS Appl. Mater. Interfaces* **3**, 2719–2725 (2011).
35. Tammy, P. C. *et al.* Hierarchically Structured ZnO Film for Dye-Sensitized Solar Cells with Enhanced Energy Conversion Efficiency. *Adv. Mater.* **19**, 2588–2591 (2007).
36. Dehong, C. *et al.* Mesoporous Anatase TiO_2 Beads with High Surface Areas and Controllable Pore Sizes: A Superior Candidate for High-Performance Dye-Sensitized Solar Cells. *Adv. Mater.* **21**, 2206–2210 (2009).
37. Zhigang, C. *et al.* Thermostable succinonitrile-based gel electrolyte for efficient, long-life dye-sensitized solar cells. *J. Mater. Chem.* **17**, 1602–1607 (2007).
38. Agarwala, S. *et al.* Investigation of Ionic Conductivity and Long-Term Stability of a LiI and KI Coupled Diphenylamine Quasi-Solid-State Dye-Sensitized Solar Cell. *ACS Appl. Mater. Interfaces* **3**, 2383–2391 (2011).
39. Flavio, S. F. *et al.* Electrochemical and Structural Characterization of Polymer Gel Electrolytes Based on a PEO Copolymer and an Imidazolium-Based Ionic Liquid for Dye-Sensitized Solar Cells. *ACS Appl. Mater. Interfaces* **1**, 2870–2877 (2009).
40. Joao, E. B. *et al.* Enhancement of photocurrent generation and open circuit voltage in dye-sensitized solar cells using Li^+ trapping species in the gel electrolyte. *Chem. Comm.* **9**, 1121–1123 (2008).
41. Yu, B. *et al.* High-performance dye-sensitized solar cells based on solvent-free electrolytes produced from eutectic melts. *Nat. Mater.* **7**, 626–630 (2008).
42. Ning, C. *et al.* N-Methyl-N-Allylpyrrolidinium Based Ionic Liquids for Solvent-Free Dye-Sensitized Solar Cells. *J. Phys. Chem. C* **113**, 4215–4221 (2009).
43. Patricia, A. H. Why does a reduction in hydrogen bonding lead to an increase in viscosity for the 1-butyl-2,3-dimethyl-imidazolium-based ionic liquids? *J. Phys. Chem. B* **111**, 4844–4853 (2007).
44. Yukihiro, Y. *et al.* Ionic Liquids Based on Dicyanamide Anion: Influence of Structural Variations in Cationic Structures on Ionic Conductivity. *J. Phys. Chem. B* **111**, 4742–4749 (2007).
45. Hiroyuki, T. *et al.* Physicochemical properties and structures of room temperature ionic liquids. 2. Variation of alkyl chain length in imidazolium cation. *J. Phys. Chem. B* **109**, 6103–6110 (2005).
46. Stephan, S. *et al.* An ionic liquid as catalyst medium for stereoselective hydrogenations of sorbic acid with ruthenium complexes. *J. Prak. Chem.* **342**, 348–354 (2000).
47. Yukihiro, Y. *et al.* Imidazolium-Based Ionic Liquids Formed with Dicyanamide Anion: Influence of Cationic Structure on Ionic Conductivity. *J. Phys. Chem. B* **111**, 12204–12210 (2007).
48. Patrick, M. *et al.* Ionic conductivity measurements of molten iodide-based electrolytes. *J. Power Sources* **160**, 752–757 (2006).
49. Fei, X. *et al.* The first crystallographic example of a face-sharing fluoroaluminate anion $Al_2F_9^{3-}$. *Dalton Trans.* **41**, 3494–3502 (2012).
50. Yanli, W. *et al.* An Evidence for the Chiral Discrimination of Naproxen Enantiomers: A Combined Experimental and Theoretical Study. *J. Phys. Chem. C* **115**, 4033–4040 (2011).
51. Bernadette, M. Q. *et al.* Novel electrochemical studies of ionic liquids. *Langmuir* **18**, 1734–1742 (2002).
52. Peng, W. *et al.* A Binary Ionic Liquid Electrolyte to Achieve ≥7% Power Conversion Efficiencies in Dye-Sensitized Solar Cells. *Chem. Mater.* **16**, 2694–2696 (2004).
53. Yiming, C. *et al.* Dye-sensitized solar cells with solvent-free ionic liquid electrolytes. *J. Phys. Chem. C* **112**, 13775–13781 (2008).
54. Ze, Y. *et al.* Investigation of Iodine Concentration Effects in Electrolytes for Dye-Sensitized Solar Cells. *J. Phys. Chem. C* **114**, 10612–10620 (2010).
55. Farouq, F. S. *et al.* Hydrogen Bonding Motifs of *N*,*N*′,*N*″-Trisubstituted Guanidinium Cations with Spherical and Rodlike Monoanions: Syntheses and Structures of I^-, I_3^-, and SCN^- Salts. *Cryst. Growth & Des.* **6**, 258–266 (2005).
56. Daesub, H. *et al.* Enhanced charge collection efficiency of dye-sensitized solar cells based on size-tunable hierarchically structured TiO_2 beads. *J. Mater. Chem. A* **1**, 1359–1367 (2013).

Acknowledgments

The authors gratefully acknowledge support from the Basic Science Research Program through the National Research Foundation of Korea (NRF, 2012045675), funded by the Ministry of Education, Science, and Technology, and the Korea Research Council of Fundamental Science & Technology (KRCF) and KIST for "National Agenda Project (NAP)" program (S.Y.J.), the KIST Institutional Programs (2E23900 and 2K02120) (D.Y.K.), and the Global Frontier R&D Program on Center for Multiscale Energy System, funded by the National Research Foundation under the Ministry of Education, Science and Technology, Korea (2013-8-2018) (D.K.). D.R.M. is grateful to the Australian Research Council for his Australian Laureate Fellowship and for funding from the Australian Centre of Excellence in Electromaterials Science.

Author contributions

D.H., D.K. and S.Y.J. wrote the main manuscript text and figure 1. D.H., D.Y.K. and S.M.J. prepared figure 2–7 and Table 1–4. V.A. and D.M. wrote parts of discussion section. All authors reviewed the manuscript.

Additional information

Supplementary information accompanies this paper at http://www.nature.com/scientificreports

Competing financial interests: The authors declare no competing financial interests.

How to cite this article: Hwang, D. *et al.* Highly Efficient Plastic Crystal Ionic Conductors for Solid-state Dye-sensitized Solar Cells. *Sci. Rep.* **3**, 3520; DOI:10.1038/srep03520 (2013).